

Active Control of Separated Flow over a Circular-Arc Airfoil

Sergio Miranda

Thesis submitted to the Faculty of the Virginia Polytechnic Institute and State
University in partial fulfillment of the requirements for the degree of

Masters of Science
In
Engineering Mechanics

Demetri P. Telionis, Chair
Dean T. Mook
Muhammad R. Hajj
Scott L. Hendricks

May 8, 2000
Blacksburg, Virginia

Keywords: Flow control, wind tunnel testing, airfoil, vortex flow

Copyright 2000, Sergio Miranda

Active Control of Separated Flow over a Circular-arc Airfoil

Sergio Miranda

(ABSTRACT)

An experimental study of active control of fully separated flow over a symmetrical circular-arc airfoil at high angles of attack was performed. The experiments were carried out in a low-speed, open circuit wind tunnel. Angles of attack from 10 to 40 degrees were tested. Low-power input, unsteady excitation was applied to the leading or trailing edge shear layers. The actuation was provided by the periodic oscillation of a 4-percent-chord flap placed on the suction side of the airfoil and facing the sharp edge. Vortex-shedding frequencies were measured and harmonic combinations selected as the applied actuator frequencies.

Pressure measurements over the airfoil show that the control increased the normal force coefficient by up to 70%. This supports the idea of vortex capture in the time-averaged sense, enhancing the lift on the airfoil by managing the shear layer roll up.

The results indicate the viability of the control of large-scale flow fields by exploiting the natural amplification of disturbances triggered by small-scale actuators.

The application of flow control on sharp-edged aircraft wings could lead to improved maneuverability, innovative flight control and weight reduction. These can be achieved by inexpensive, low-power, rugged actuators.

Dedication

*To my fiancé Carolina. You did this with me...even from so far away...Te amo~~~!!!
and my parents, who always encouraged and supported me to achieve my dreams.*

Acknowledgements

The list is endless if I have to thank all the people that made possible this work. My first and sincere thanks goes to the mastermind of all I have done: Dr. D. P. Telionis. He gave me the possibility of studying in the United States and showed me what I thought nobody could really do: that there are no limits on what we can achieve. We agreed in many things, disagreed in others, but there was no time where I could not learn something from him. He supported me from the beginning and never said no to a new idea. Thanks, from the bottom of my heart.

The other person who I owe an immense gratitude is my laboratory fellow and friend Matthew Zeiger. He was with me on the worst times of my research, helping with the pressure acquisition system that he best knows. Thanks for your time and friendship. I'll try to catch up on you in golfing...

Working in the ESM Fluids Laboratory allowed me to meet many people, graduates, undergraduates and technicians. All of them helped me on building this brick by brick project, and all of them showed me that friendship doesn't have frontiers. Mark Carrara, Alexis Telionis, Michael Tadema-Wielandt, Demetri Stamos, Pavlos Vlachos, Robert Hodges, Sandra Klute, Yasser El-Okda. I will never forget you guys.

Friends outside the Lab helped me to forget my research difficulties and enjoy my life. All of them participated in this thesis, by relaxing me in the anger times. A special thanks to my friend and roommate Juan Salcedo, for his friendship and taking me out of the lab when I most needed it. I can not forget to mention Diego de la Riva, Axel Castaños, Valerio Viti and all the people I have met in the Latin American and Iberic Student Association, LAIGSA.

I could never forget to mention Dr. D. T. Mook. I had the pleasure to know him as a professor and also as a graduate committee advisor. His comments were always more than helpful. I really enjoyed those afternoons of spanish conversations.

I also want to thank Dr. M. R. Hajj and S. L. Hendricks for integrating my committee and spending their valuable time for me. I had the pleasure to meet them as a teaching assistant, and respect them for their simplicity and wisdom.

The Engineering Science and Mechanics department would not be the same without Loretta Tickle. She was the solution for all the problems, and she solved each of them efficiently. She puts her heart on everything she does, and I will never forget that. Thank you.

A brief, but more than important thanks goes to Dr. Martinez. You know why...

I don't want to forget my family, the old one, and the new one (in law's). All of you helped me to be here, and e-mails counting can probably show it. Thanks for your love.

At last, but not least, I want to thank the one that made everything possible, from the very beginning. I owe you this beautiful life, and my love for everything I do. You know I do my best. Thank you God.

Table of Contents

TABLE OF FIGURES AND MULTIMEDIA OBJECTS	VIII
NOMENCLATURE	XIII
CHAPTER 1 INTRODUCTION	1
1.1 Flow control	2
1.2 Separated Flow	5
CHAPTER 2 REVIEW OF BASIC CONCEPTS	7
2.1 Physics of Enhancing Vortex Lift by Unsteady Excitation	8
2.1.1 Vortex layer instability-receptivity	9
2.1.2 Resonance	11
Sound-Vortex Resonance	12
Vortex-Vortex Resonance	12
2.1.3 Streaming	13
Acoustic Streaming	13
Vortical Streaming	14
CHAPTER 3 LITERATURE REVIEW	15
3.1 Relevant Previous Work	15
3.2 Conclusions	32
CHAPTER 4 EXPERIMENTAL SETUP AND EQUIPMENT	34
4.1 Introduction	34
4.2 Wind Tunnel	34
4.3 Airfoil model and instrumentation	36
4.3.1 Airfoil Model	36
4.3.2 Actuation System	40
4.3.3 Feedback Sensor	42
4.3.4 Strain Gage Balance	44

4.3.5 Pitot Rake	49
4.4 Data Acquisition System and Additional Instrumentation	52
CHAPTER 5 EXPERIMENTAL RESULTS	55
5.1 Rake Calibration and Positioning	55
5.2 Data Acquisition Process	58
5.3 Results	64
5.3.1 Base flow	64
5.3.2 Controlled Case	70
5.4 Balance Results	90
CHAPTER 6 CONCLUSIONS AND PROPOSED WORK	94
REFERENCES	96
VITA	99

Table of Figures and Multimedia Objects

Figure 1.1.1 Classification of flow control strategies (from Gad-el-Hak, 1998)	3
Figure 1.1.2 Different control loops for active flow control (from Gad-el-Hak, 1998)	4
Figure 1.2.1 Separated/Separating Flows and possible actuation	5
Figure 2.1 The mean $C_L \sim \alpha$ of a flat plate. From Wicks (1954) (Taken From Wu's paper)	7
Figure 2.1.1.1 Sketch of initial mixing layer. From Ho and Huerre (1984). (Taken From Wu's paper)	9
Figure 2.1.1.2 Variations of normalized amplification rate of the perturbed free vortex layer. From Ho and Huerre (1984) (Taken From Wu's paper). Linear stability theory: — $R = 1$; — · — $R = 0.5$; - - - $R \ll 1$. Experiments: 7 , $\lll R = 1$; x $R = 0.72$; D $R = 0.31$.	10
Figure 2.1.1.3 Subharmonic and vortex merging. From Ho (1981)(Taken From Wu's paper).	10
Figure 3.1 Vortex-generator test configurations shown approximately to scale. From Bursnall (1952).	16
Figure 3.2 Sketch of testing model. From Zhou <i>et al</i> (1993).	17
Figure 3.3 Variation of lift coefficient with forcing frequency. $\alpha = 27^\circ$, $Re = 6.65 \times 10^5$. From Zhou <i>et al</i> (1993).	18
Figure 3.4 Distribution of pressure coefficient. $\alpha = 27^\circ$, $Re = 6.65 \times 10^5$. From Zhou <i>et al</i> (1993).	18
Figure 3.5 Relation between vortex shedding frequency and forcing frequency. $\alpha = 27^\circ$, $Re = 6.71 \times 10^5$. From Zhou <i>et al</i> (1993).	19
Figure 3.6 Turbulence energy in the wake. y' is the vertical distance in the wind-tunnel coordinates, with $y' = 0$ at the leading edge of the airfoil. $\alpha = 27^\circ$, $Re = 6.71 \times 10^5$, $x/c = 1.615$. Open symbols: unforced; closed: forced with $f = 2$. From Zhou <i>et al</i> (1993).	19
Figure 3.7 Mean velocity profile in the wake. y' is the same as in Figure 3.6, $\alpha = 27^\circ$, $Re = 6.71 \times 10^5$, $x/c = 1.615$, $z/c = 0.15$. Open symbols: unforced; closed: forced with $f = 2$. From Zhou <i>et al</i> (1993).	20

- Figure 3.8** a) Schematic of experimental arrangement, b) coordinate system of the flap motion, and c) oscillating mode shapes of the flap motion. From Hsiao *et al* (1998). 22
- Figure 3.9** Variation of normalized lift coefficients over an airfoil with excitation frequency at different angles of attack for $Re = 3.0 \times 10^5$ and forcing at a 1.25% chord. Arrow indicates bigger C_l/C_{l0} , with the base positioned at $C_l/C_{l0} = 1$. From Hsiao *et al* (1990). 23
- Figure 3.10** a) Maximum velocity fluctuation; b) the corresponding sound pressure level at the slot exit; and c) the lift coefficient at constant driven voltage and AOA = 22°. From Chang *et al* (1992). 24
- Figure 3.11** a) Maximum velocity fluctuation; b) the corresponding SPL; and c) the lift coefficient at AOA = 22° and driven by a low-frequency loudspeaker. From Chang *et al* (1992). 25
- Figure 3.12** Airfoil pressure distributions with and without excitation for angles of attack : a) 26° and b) 28°. From Hsiao *et al* (1994). 26
- Figure 3.13** Schematic diagram of a synthetic jet. From Crook *et al* (1999). 27
- Figure 3.14** Experimental set-up for active control of stalled flow around an airfoil by impinging vortex rings. From Kiya *et al* (1999). 28
- Figure 3.15** a) Flow visualization of the separated flow affected by the impinging vortex rings. Flow is from left to right. The phase-averaged reattachment position is indicates by the open triangles. Coordinates of position of the vortex rings are denoted by the solid triangles on the x and vertical y axes; b) Phase-averaged velocity distributions \tilde{q} in the separated flow affected by the impinging vortex rings. The phase-averaged reattachment position is indicated by the open triangles. Coordinates of position of the vortex rings are denoted by the solid triangles on the x and y axed. Thin solid lines indicate the distributions of the time-averaged velocity \bar{q} in the undisturbed shear layer, while the solid lines show the center o the shear layer. 30
- Figure 3.16** $f_a/f_s = 0.5$, $C_m = 2.5\%$, with $C_m = |v|_{max} l/U_\infty c \sin \alpha$ being $l = 2.5\% c$ and $|v|_{max}$ the maximum perturbation velocity. a) Instantaneous lift and drag coefficients. b) Power spectral density of Cl. 31
- Figure 3.17** As Figure 3.16 but $f_a/f_s = 2$. 32

Figure 4.2.1 ESM Wind Tunnel. From Seider (1984)	35
Figure 4.3.1.1 Airfoil model dimensions (inches)	38
Figure 4.3.1.2 Model geometry and pressure taps location	39
Figure 4.3.1.3 Pressure taps construction	39
Figure 4.3.1.4 32 Channel PSI ESP Pressure Scanner	40
Figure 4.3.2.1 Flap close up view	41
Figure 4.3.2.2 Flap Detail	42
Figure 4.3.2.3 High current adjustable voltage regulator	43
Figure 4.3.3.1 Complete model schematic	44
Figure 4.3.3.2 Complete airfoil model	45
Figure 4.3.3.3 Close up view of the actuating/sensing mechanism	45
Figure 4.3.4.1 Strain Gage Balance	46
Figure 4.3.4.2 Strain gage balance	47
Figure 4.3.4.3 Balance/Wing system and degrees of freedom.	48
Figure 4.3.4.4 Universal joint exploded view.	49
Figure 4.3.5.1 Pitot Rake Positioning	51
Figure 4.3.5.2 Pitot Rake	51
Figure 4.4.1 Schematic diagram of the experimental set up	53
Figure 5.1.1 Circular cylinder positioning for rake calibration	55
Figure 5.1.2 Frequency spectrum on the rake for $V_{\infty} = 16.2$ m/sec	56
Figure 5.1.3 Comparison of results for circular cylinder vortex shedding	57
Figure 5.1.4 Vortex shedding visualization for rake alignment, $U_{\infty} = 6.5$ m/s ;a) Angle of attack 50° , b) Angle of attack 30° .	59
Figure 5.2.1 Schematic of flap positions tested. a) Leading edge flap; b) trailing edge flap.	60
Figure 5.2.2 Pressure taps measured in the experiment.	62
Figure 5.3.1.1 Airfoil pressure coefficient distribution at different angles of attack. Suction and pressure sides. No actuation. For Reynolds number, see Table 5.2.1.	64
Figure 5.3.1.2 Power spectrum density on the rake for pitots 1 through 3. Angle of attack 20° . $U_{\infty} = 17.5$ m/s	66
Figure 5.3.1.3 Power spectrum density on the rake for pitots 4 through 6. Angle of attack 20° . $U_{\infty} = 17.5$ m/s	66

Figure 5.3.1.4 PSD at angles 40° through 25°. Pitot 3. Reynolds number and freestream velocity as in Table 5.2.1. PK: peak values.	67
Figure 5.3.1.5 PSD at angles 20° through 10°. Pitot 3. Reynolds number and freestream velocity as in Table 5.2.1. PK: peak values.	67
Figure 5.3.1.6 Base flow normal force coefficient with respect to time at different angles of attack. Freestream velocity and Reynolds number from Table 5.2.1. Avr: average value.	69
Figure 5.3.2.1 Normal force coefficient variation with excitation frequency. Angle of attack: 40°; □ leading edge flap actuation; △ trailing edge flap actuation.	71
Figure 5.3.2.2 Strouhal number variation with excitation frequency. Angle of attack: 40°; □ leading edge flap actuation; △ trailing edge flap actuation.	71
Figure 5.3.2.3 Normal force coefficient variation with excitation frequency. Angle of attack: 30°; □ leading edge flap actuation; △ trailing edge flap actuation.	72
Figure 5.3.2.4 Strouhal number variation with excitation frequency. Angle of attack: 30°; □ leading edge flap actuation; △ trailing edge flap actuation.	72
Figure 5.3.2.5 Normal force coefficient variation with excitation frequency. Angle of attack: 25°; leading edge flap actuation.	73
Figure 5.3.2.6 Strouhal number variation with excitation frequency. Angle of attack: 25°; leading edge flap actuation.	73
Figure 5.3.2.7 Normal force coefficient variation with excitation frequency. Angle of attack: 20°; □ leading edge flap actuation; △ trailing edge flap actuation.	74
Figure 5.3.2.8 Strouhal number variation with excitation frequency. Angle of attack: 20°; □ leading edge flap actuation; △ trailing edge flap actuation.	74
Figure 5.3.2.9 Normal force coefficient variation with excitation frequency. Angle of attack: 15°; leading edge flap actuation.	75
Figure 5.3.2.10 Strouhal number variation with excitation frequency. Angle of attack: 15°; leading edge flap actuation.	75
Figure 5.3.2.11 Normal force coefficient variation with excitation frequency. Angle of attack: 10°; leading edge flap actuation.	76
Figure 5.3.2.12 Strouhal number variation with excitation frequency. Angle of attack: 10°; leading edge flap actuation.	76
Figure 5.3.2.13 PSD of pitot 3 at excitation $ F =2.06$. Angle of attack 30°	78
Figure 5.3.2.14 PSD of pitot 3 at excitation $ F =1.75$. Angle of attack 25°. Pk: peaks.	79

Figure 5.3.2.15 Pressure coefficient distribution for controlled case. Angle of attack 20°. Leading edge excitation.	80
Figure 5.3.2.16 PSD of pitot 3 for controlled case. Angle of attack 20°. Leading edge excitation.	81
Figure 5.3.2.17 Evolution of normal force coefficient for different actuation frequencies. Angle of attack 20°. Leading edge excitation.	82
Figure 5.3.2.18 Pressure coefficient distribution for controlled case. Angle of attack 20°. Trailing edge excitation.	83
Figure 5.3.2.19 PSD of pitot 4 for controlled case. Angle of attack 20°. Trailing edge excitation.	83
Figure 5.3.2.20 Evolution of normal force coefficient for different actuation frequencies. Angle of attack 20°. Trailing edge excitation.	84
Figure 5.3.2.21 Pressure coefficient distribution for controlled case. Angle of attack 15°. Leading edge excitation.	85
Figure 5.3.2.22 PSD of pitot 3 for controlled case. Angle of attack 15°. Leading edge excitation.	86
Figure 5.3.2.23 Evolution of normal force coefficient for different actuation frequencies. Angle of attack 15°. Leading edge excitation.	86
Figure 5.3.2.24 Pressure coefficient distribution for controlled case. Angle of attack 10°. Leading edge excitation.	88
Figure 5.3.2.25 PSD of pitot 3 for controlled case. Angle of attack 10°. Leading edge excitation.	89
Figure 5.3.2.26 Evolution of normal force coefficient for different actuation frequencies. Angle of attack 10°. Leading edge excitation.	89
Figure 5.4.1 Natural frequency spectrum for the balance system.	91
Figure 5.4.2 Integrated pressure over the suction side of the airfoil. $\alpha = 30^\circ$, $U_\infty = 10 \text{ m/s}$.	92
Figure 5.4.3 Balance output voltage for the lift channel. $\alpha = 30^\circ$, $U_\infty = 10 \text{ m/s}$.	92
Table 5.2.1 Experiment parameters on the airfoil testing. LE: leading edge; TE: trailing edge	62
Table 5.2.2 Pressure taps location	63

Nomenclature

θ	Flap angle
L	Lift
ρ	Flow Density
Γ	Circulation
q	Shear layer thickness
\mathbf{a}_i	Imaginary part of the complex wave number
C_l	Section lift coefficient
C_p	Pressure coefficient
C_n	Section normal force coefficient
U	Velocity / Velocity on the shear layer
c	Airfoil Chord
f	Frequency
P	Pressure
α	Angle of attack
$ F $	Reduced frequency $\equiv f_a / f_s$
$ Str $	Normalized Strouhal number $\equiv Str / Str_0$
$ C_n $	Normalized section normal force coefficient $\equiv C_n / C_{n0}$

Subscripts:

<i>stall</i>	Static stall condition
∞	Free stream
<i>a</i>	Actuator
<i>s</i>	Shedding
<i>suc</i>	Airfoil suction side
<i>pres</i>	Airfoil pressure side
0	Base case, no control applied.

Chapter 1 Introduction

Over the past few decades, there has been a marked trend towards the design of fighter aircraft with low radar signature and at the same time capable of flying at supersonic regimes, maintaining high levels of maneuverability. This kind of configurations involve many physical and technical limitations, setting a new challenge to the industry.

Sharp edges are a common feature on these airframes, and separation can not be avoided for even low angles of attack. The need for complex flap systems or swept wing configurations with stable lifting vortices is part of the tools that designers use to achieve high levels of agility and also flight at angles of attack well beyond the maximum lift.

Flow control is a new approach in the design of new radical configurations. The suction side of the wings for low-observable fighter aircraft is dominated by separated flow that comprises of large and small vortices with a wide spectrum of length scales and frequencies. Active control of this vortical structure could serve for different purposes at different flight regimes and angles of attack. Recent experimental and numerical evidence shows that at high angles of attack, it is indeed possible to increase lift by as much as 70 percent by controlling the vortex forming process of separated flows. This can be achieved by utilizing low power actuators, effectively controlling the shear layer roll up over the wing.

The system could provide an effective way of aerodynamic controls reducing or eliminating the required moving surfaces, or trimming the aircraft without incurring an increase of drag. This could lead to an important reduction in take off weight and airframe simplicity. It is also possible to permit the aircraft to fly efficiently at post-stall angles of attack, improving turn performance in air combat. The structures could benefit by this new approach as well. Buffeting control may reduce the airloads, leading to a possible reduction of the structure weight and also having a deep impact on the life on the airframe. All these could be implemented via fast computers that permit the management of multiple feedback parameters present in the control of the flow field over these configurations.

The goal of this research is to get a better insight into the flow field over these configurations, and analyze the effects of the control on the aerodynamic characteristics. A two-dimensional circular-arc airfoil is chosen as the test bed for the analysis of flow control at high angles of attack. This is a necessary step for the understanding of the vortex lift augmentation control on the subsonic regime of supersonic, stealth wing configurations. Attached flow can not be sustained over a sharp edge leading edge even at low angles of

attack. A different means of flow control has to be put in practice: flow control of separated flows.

Before proceeding further, we provide here a short description of the concepts of flow control.

1.1 Flow control

Man has never been satisfied with the world that surrounds him, and tried to control or improve it from the very beginning to get more beneficial effects. This applies to almost all science disciplines nowadays, and fluid Mechanics is not an exception. Since early times, fluid was an attractive and at the same time difficult to understand subject that forced investigators to improve their skills and knowledge. Even after understanding some of the complicated fluid behavior investigators were never satisfied, and put also their efforts on controlling it. That's where the discipline of Flow Control was born.

It is hard to provide a definition for flow control, but one that could closely fit with this work is given by Fiedler (1998): "...is a process or operation by which certain characteristics of a given flow are manipulated in such a way as to achieve improvements or a specific technical performance".

This definition of flow control is bounded by the fact that this manipulation is effectuated by "...the internal amplification of a small 'tailored; disturbances". The word 'control' might seem too strict or even arrogant in the sense that the flow is just induced to behave in a given form. This control is just a triggering of the natural unsteadiness by means of a low power actuator. In such a way that the flows develops naturally in the desired form.

An excellent introduction and historical perspective of flow control can be found in Gad-el-Hak (1998). From there, we can make use of two figures that show where we stand in this research in terms of the applied control. Figures 1.1.1 and 1.1.2 show the flow control strategies and feedback loops for different forms of actuation. Figure 1.1.1 basically provides the distinction between passive and active actuation and the active different classifications. The active control differs from the passive in the sense that auxiliary power is required. The reactive active control is that one where a control signal is taken from measurements of the flow, whereas in the predetermined case, the control is not dependent on the flow condition. Reactive flow itself divides in feedforward, where the measured variable and the controlled variable differ (applying a control law); and feedback,

where the controlled variable is measured, fed back, and compared with a reference input. The feedback reactive control is also subdivided in different control methods.

The possible control loops are depicted in Figure 1.1.2. a) shows a typical predetermined active control strategy, being an open loop. The reactive active flow control can be an open feedforward loop as in b) or a closed feedback one as in c). As we will see later, the control loop used in this work is of the reactive active type, using an open feedforward control loop.

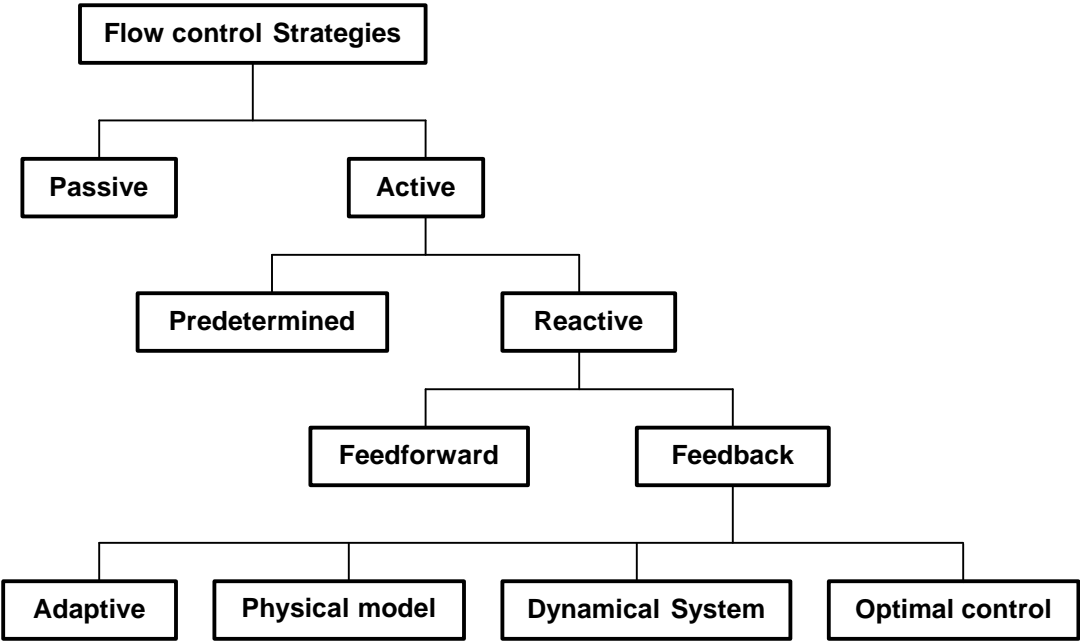


Figure 1.1.1 Classification of flow control strategies (from Gad-el-Hak, 1998)

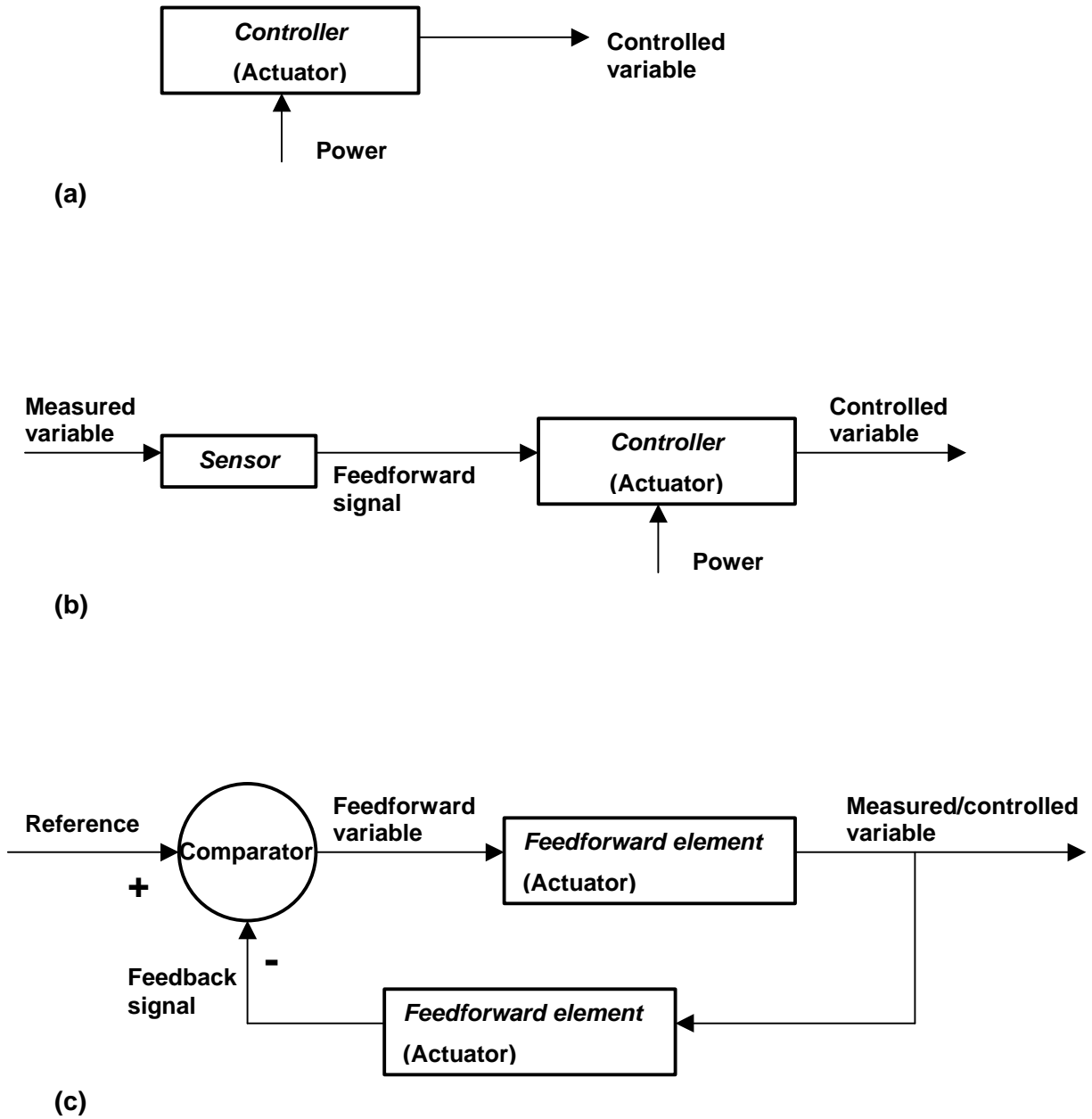


Figure 1.1.2 Different control loops for active flow control (from Gad-el-Hak, 1998)

1.2 Separated Flow

Our goal is to be able to control the separated flow over a thin circular-arc airfoil. For that matter, we should clarify here the difference between separated flow control and flow separation control. Both imply the condition of a detached flow, but in a different flow scale. Fiedler (1998) makes a clear distinction between these two flow fields. This is shown in Figure 1.2.1.

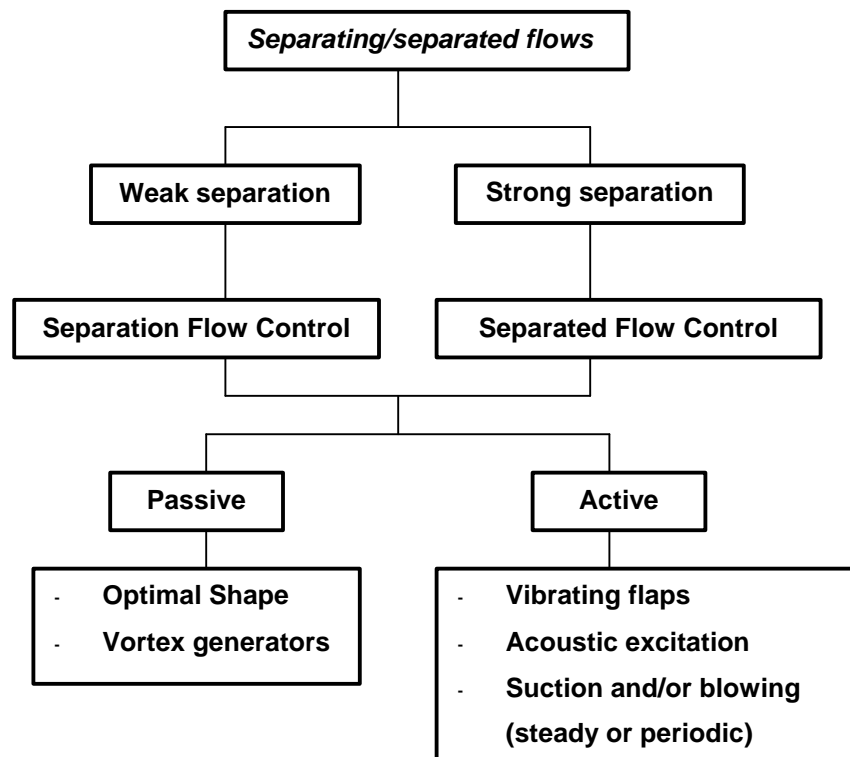


Figure 1.2.1 Separated/Separating Flows and possible actuation

Weak separation can be defined as that one where the separation point is variable or undefined. That is the case for most flow fields around airplanes (ex: flow over a wing), where the separation point depends solely on the surface contour and flight condition. When separation occurs, the wall boundary layer detaches from the wall and develops into

a free shear layer. Since the free shear layer is more susceptible to control than the boundary layer itself, any attempt of control has to introduce a perturbation directly into it.

The strong separation case is the one where the separation point is fixed. This is the one that applies to this work, and to mostly all bluff bodies with sharp corners. The separation point is usually fixed at a sharp edge or corner.

For both the strong and weak separation cases, passive and active controls are possible. The latter is less effective and more compromising. The shape is optimized to one flight regime, and can not be changed, unless leading and trailing edge flaps are used¹. In the case of bluff bodies, passive control has a more limited application, influencing the flow in a reduced way.

Active control, has shown to be more effective and flexible in its application. It is also not as intrusive as vortex generators, and can produce substantial increases in L/D. Various practical means of applying active control are shown in Figure 1.2.1. All of these have been experimentally explored and shown to yield different results.

In the specific case of airfoils aerodynamics, it is important to notice that this classification depends on the leading edge radius. For sharp leading edges, the airfoil is going to behave as a bluff body even for the low α range. This is because there is an immediate separation due to the large unfavorable pressure gradient existing at the sharp edge. This separation is normally prevented by the use of leading edge flaps.

For rounded leading-edge airfoils, the weak or strong separation classification depends strictly on the angle of attack. Wu *et al.* (1998) make a nice distinction between these two cases, and this is how Figure 1.2.1 also classifies the conditions. For the angle of attack range $\alpha < \alpha_{stall}$, the flow is not fully separated, and the control is aimed at overcoming separation. Usually the result is the complete elimination of the separated flow at a given α or the reattachment of the flow downstream, creating a recirculating bubble. For $\alpha > \alpha_{stall}$ the flow is fully separated, and is most uncertain that the control will promote reattachment. This defines two control categories: *separation control* and *separated flow control*.

This research falls into the category of active control of a strong separation, ie. separated flow control. The actuation is applied by means of an oscillating flap either on the leading or trailing edge.

¹ New materials are giving the possibility of modify the wing shape in flight to achieve the optimized condition. This are the so-called smart wings, modifying camber and thickness as required.

Chapter 2 Review of Basic Concepts

The area of separated flow control is full of empirical relations and physical interpretations, but a theory that could back up all experiments performed to the date is still missing. This is due to the complexity of the flow, and its highly non-linear behavior. An excellent review and starting point for this kind of flow control is given by Wu *et al.* (1991), who discuss the maximum lift achieved at super high angles of attack, and the aircraft maneuvering possibilities that this opens. They show how a simple flat plate has a second maximum lift peak at a very high angle of attack, as shown in Figure 2.1.

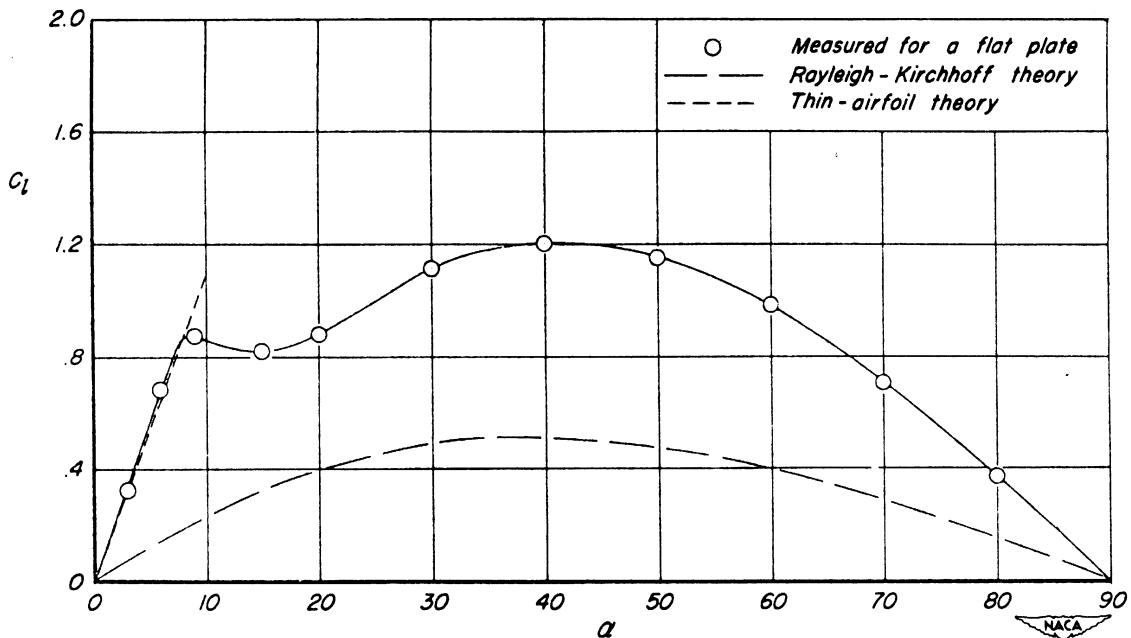


Figure 2.1 The mean $C_L \sim \alpha$ of a flat plate. From Wicks (1954) (Taken From Wu's paper)

The idea is to break through the unsteady separation barrier by enhancing the flow separation and unsteadiness in a controlled manner using unsteady excitation. This would lead to the third generation of aeronautical types of flow, with weakly unsteady detached vortex flow.

The overall idea is to increase lift by capturing a vortex in the suction side of the wing in the average sense. The Kutta-Joukowski lift formula relates the lift with the amount of circulation around the wing by:

$$L = -r U \Gamma$$

If a vortex is captured in the average sense, an increase in lift will be induced due to the additional circulation around the airfoil. In order to create an increment in lift, there can not be counter rotating vortices over the airfoil, since this would destroy any total circulation. This means that if a strong vortex over the wing can't be sustained, then vortex shedding must exist. Should the vortex shedding be completely controlled or eliminated? Not necessarily: vortex shedding can exist if in the average a non-zero circulation is generated. Wu *et al* (1991) discuss different experiments done in the past and how they tried to achieve the vortex lift by different means. They emphasize the fact that in the 2-D experiments, the vortex is unstable and has the tendency to become three-dimensional. The only possible way to stabilize the vortex is by inducing a strong axial velocity in the spanwise direction. This is how slender wings can maintain a stable vortex on their leading edges without control, since the vortex generated has a strong core axial velocity. They don't need flow control since this is the natural way the vortex appears in this kind of flow, in its stable state. Anyway, if angle of attack is highly increased on a slender wing, vortex shedding occurs, detaching the vortices unsteadily from the upper surface. This would repeat again the behavior observed in the 2-D case for even lower angles of attack. The difference is that in the 2-D case, a stable vortex can't exist, and detaches immediately. But it is important to notice that even when the flow field over a 2-D airfoil and a slender wing are completely different, there are still analogies between them for high angles of attack.

Different theoretical models were tried without real application to the vortex capture phenomenon. This problem is difficult to model, involving a strong nonlinear interaction and unsteadiness of thin vortex layers and shed vortices.

2.1 Physics of Enhancing Vortex Lift by Unsteady Excitation

In the same paper, Wu *et al* (1991) summarize the physics of the vortex lift enhancement by unsteady excitation. This can be resumed in a chain of events:

vortex layer instability-receptivity-resonance-streaming

These are the mechanisms that take place in the flow field and need to be understood in order to devise an effective method to control the flow and capture a vortex.

2.1.1 Vortex layer instability-receptivity

When the flow separates on a smooth surface or sharp edge, the main product is the continuous shedding of vorticity in the form of a shear layer. This is the building brick of the flow field and the one that can be eventually controlled by introducing perturbations. It is already known that straight shear layers are unstable to small perturbations (Kelvin-Helmholtz instability). Experiments have shown that there is a most amplified perturbation frequency corresponding to a Strouhal number

$$St = \frac{f \mathbf{q}}{\bar{U}} \approx 0.032x(1 \pm 5\%)$$

for the full range of $0 \leq R \leq 1$, where $R = (U_1 - U_2)/2\bar{U}$ and $\bar{U} = U_1 + U_2$. (Figures 2.1.1.1 and 2.1.1.2).

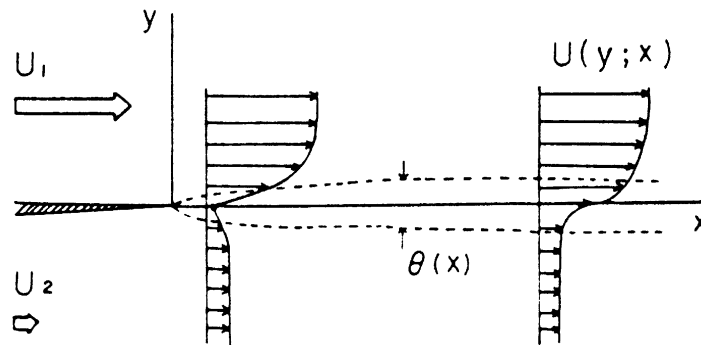


Figure 2.1.1.1 Sketch of initial mixing layer. From Ho and Huerre (1984). (Taken From Wu's paper)

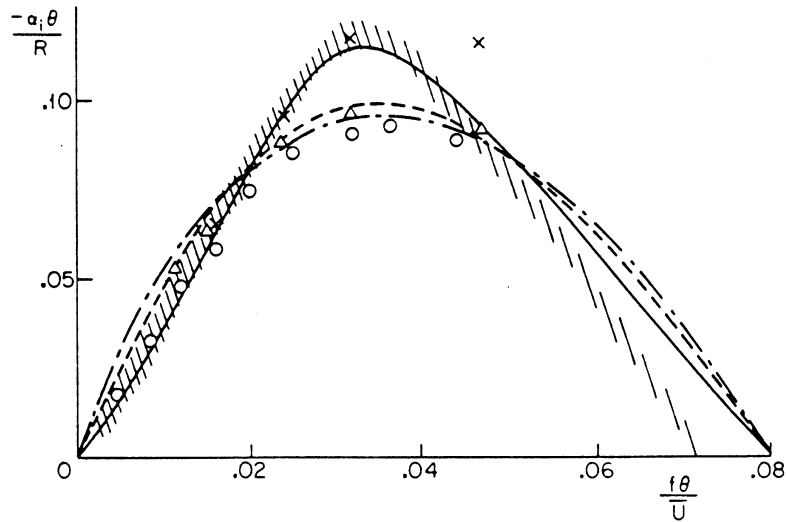


Figure 2.1.1.2 Variations of normalized amplification rate of the perturbed free vortex layer. From Ho and Huerre (1984) (Taken From Wu's paper). Linear stability theory: — $R = 1$; — · — $R = 0.5$; - - - $R \ll 1$. Experiments: \circ $R = 1$; \times $R = 0.72$; \diamond $R = 0.31$.

As the vortex layer evolves, it rolls up into vortices which soon start interacting with each other. The sub-harmonic instability plays its role, causing the vortex merging at half the fundamental frequency with double wave length. This is shown in Figure 2.1.1.3.

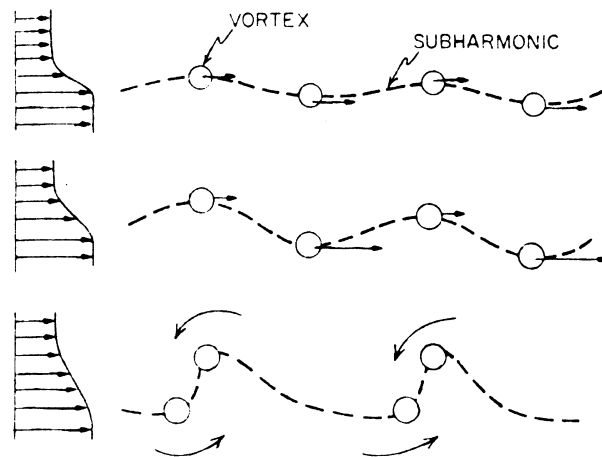


Figure 2.1.1.3 Subharmonic and vortex merging. From Ho (1981)(Taken From Wu's paper).

The process goes on repeating this behavior, doubling the vortex size each time and increasing the layer thickness. This describes the local interaction of the vortices. A global effect is produced due to the upstream influence of the downstream stronger concentrated vortices. This is called feedback mechanism and adds its effects to the local instability.

Vortex pairing and the growth of shear layers are strongly affected by small external excitation. This is the receptivity problem: how certain modes are excited by imposed disturbances. Depending on the forcing frequency, the response frequency of the shear layer will set to a particular harmonic. The important fact is that very low forcing levels ($0.01 - 0.1\% \bar{U}$) are needed if the forcing frequency is properly chosen.

The application of a straight vortex layer is practically of no use in the present case, since the shear layer will be a rolled-up one. However, the fundamental behavior of the rolled-up and straight vortex layer is similar, and stability and receptivity fundamentals can be interpolated from the latter.

2.1.2 Resonance

The concept of resonance here is closely related to the one known from simple oscillation theory. If the forcing terms on a linear oscillator have the same frequency as that of the fundamental mode of the linear oscillator, then an internal resonance appears and leads to an enhanced response. The resonant response of this oscillation, might be favorable or not, and if the former is encountered, then due to the amplification and organizing effects of the internal resonance it provides a potential for managing the unsteady detached flow.

Since the resonance is the result of the interaction of two periodic events synchronized in phase with frequencies that are integer multiples of each other, we need a periodic flow feature and feedback mechanism which is in phase with the former in order to enable the disturbance to interact to itself. In this form, with a low power input and using the natural frequency of the system, the amplitude of the excitations can be greatly improved. For our application, the resonance of interest is the wave-vortex resonance. The waves include:

- Sound waves, being longitudinal acoustic/shock waves, generated from normal perturbations in unsteady processes.
- Vortex waves, being transverse vortical waves, generated from tangential perturbations in unsteady processes.

Both cases are inherently coupled, especially in the proximity to solid surfaces. Then, in order to control the vortex layer development and create favorable resonance, both acoustic waves and vortex waves can be imposed as forcing sources. Wu *et al.* (1991) provide an extensive review of the physics of both cases. The main important points are presented below.

Sound-Vortex Resonance

This appears as the resonant interaction of acoustic field and vortical waves in separated vortex layers. Many experiments were performed, and they all show that in separated flows with sound resonance, good spanwise vortex shedding correlation is obtained, and great concentration of vorticity. Even when unsteady vortex flow is the principal generator of acoustic waves, the inverse is not true. In order to create the resonant condition, there has to be a mechanism by which the normal pressure fluctuations transfer to tangential pressure fluctuations creating the feedback mechanism. This process is found to be realized in the wall trough the adherence condition. The sound-vortex interaction effects the following benefits:

- Allows to set the frequency of unsteady vortex layer evolution
- Presents a natural means of organizing the vortical flow structure
- Possibility of obtaining the most enhanced vortical flow with the least amount of energy.

The most interesting part in the mechanism of sound-vortex interaction, is that Kutta condition imposed on sharp edges enhances the mechanism of energy transfer from acoustic field to the vortex layer or viceversa. Analytical and experimental results show that sharp edge leading and trailing edges enhance the sound-vortex resonance. In both cases, the optimum was found, placing the sound source as close to the edge and with the acoustic waves emanating to the edge off the airfoil.

The sound-vortex resonance is a very flexible system to apply since it can produce a wide range of frequencies (20 Hz to 30 kHz) and was found to convert 99% of the incident acoustic energy to vortical energy at resonant frequencies.

Vortex-Vortex Resonance

A mechanical oscillation, as the one implemented in this experiment, produces a vortical wave that can generate vortex-vortex resonance. Since there is no need for transformation from normal waves to tangential waves, the vortex-vortex interaction is

more straightforward and leads to better vortex shedding frequency fixing. The drawback is that the frequency range is more limited (110 Hz for this experiment). The simplest explanation is that the tangential oscillation to the surface produces vortical waves that establish the vortex-vortex resonance. There are also acoustic waves generated in the process.

It is important to notice that research has shown that oscillating sharp edges are more effective than oscillating bluff bodies (see Wu *et al*, 1991). This is due to the fact that from a sharp edge the separation is fixed and also the vorticity besides being more concentrated, has the same sign (compared to a Karman vortex that alternates vortices signs). This results in less oscillation amplitude needed to achieve the same effect. There is no systematical theoretical explanation to the vortex-vortex resonance mechanism. Anyway, experiments show that using proper forcing frequency (by means of flaps, synthetic jets, etc) results are better than those produced by acoustic excitation, even when the resonant condition is not arrived at.

The best of both worlds can probably be achieved by blowing/suction. Both vortex and acoustic waves are generated in the process, and this probably explains the effectiveness achieved in the experiments.

2.1.3 Streaming

We were able to see that the internal resonance can excite and enhance the well organized vortical waves. This doesn't mean though that the overall effect creates a lift increment. To achieve this, the alternating change of sign of the shed vortices has to be managed in order to make the net time-averaged circulation non-zero. The definition of streaming or drift motion comes from the mean motion of a fluid from the nonlinear wave interaction. As before, we have two forms of streaming due to each wave-vortex resonance: acoustic streaming and vortical streaming.

Acoustic Streaming

The acoustic streaming can be best understood as the effect of the nonlinear Reynolds stress in a periodic flow. The necessary mechanism which dissipates the wave energy converting it into steady streaming, is the viscosity. That means that it is a nonlinear result of the sound-vortex interaction.

It can be shown that the product of the acoustic streaming is vortical flow, therefore, under given conditions, the acoustic generation can be seen as a steady vorticity source. There is no theoretical work that analyzes the effect of acoustic streaming on the evolving vortex layer, but the experiments and understanding of the physics show that this is effective in generating organized vortical flows.

Vortical Streaming

Vortical streaming is the vortex flow induced by an incident vortical wave. Like acoustic streaming, for a vortical streaming to be strong, there must be an effective mechanism to attenuate the vortical wave and convert its energy to the main vortex. For incompressible flows, the mechanical dissipation that augments streaming is viscosity.

Chapter 3 Literature Review

The area of airfoil research is broad and full of interesting results. Nevertheless, flow control experiments over separated flow found usually applies only for low speed, low Mach number conventional airfoils. Experiments performed over supersonic airfoil configurations, even in the low speed regime, are not available. It's not strange, since active flow control is a relatively newcomer to the field.

3.1 Relevant Previous Work

Some declassified literature is available from research done on the early fifties, on the very beginning of the supersonic flow era. Even in those days, flow control was in the mind of researchers and engineers, knowing that a sharp leading edge, appropriate for supersonic flow performed poorly on subsonic regimes. A good indication of that interest is given in the paper by Bursnall (1952). In his paper, Bursnall tried to increase the maximum lift of a 6 percent symmetrical circular airfoil by means of vortex generators. Tests were performed in the Langley Low Turbulence tunnel, at a Reynolds of 2×10^6 and Mach numbers below 0.2. Different configurations were tested on his experiments, and none of them showed a substantial increase in lift, being the greatest one achieved of 0.1 of ΔC_l . That corresponds to only a 12 percent increase in lift. Figure 3.1 shows the different vortex generators configurations tested.

Even when the generators decreased the extent of the local separation from the leading edge at lower angles of attack, the majority of them were enveloped by the separated region just below stall. Not even the vortex generators swept forward of the leading edge, were enough to produce a favorable effect on the flow field. It must be noticed also that the main goal was to force reattachment over the suction side of the airfoil by mixing the high-energy air of the main stream and the low-energy air in the separated region. This entrainment effect is performed utilizing the induced vortex generated at the tip of the small lifting airfoil (vortex generator); a complete different concept to the one proposed in this research. This is one clear indication that passive flow control of separated flow on these configurations is practically of no use.

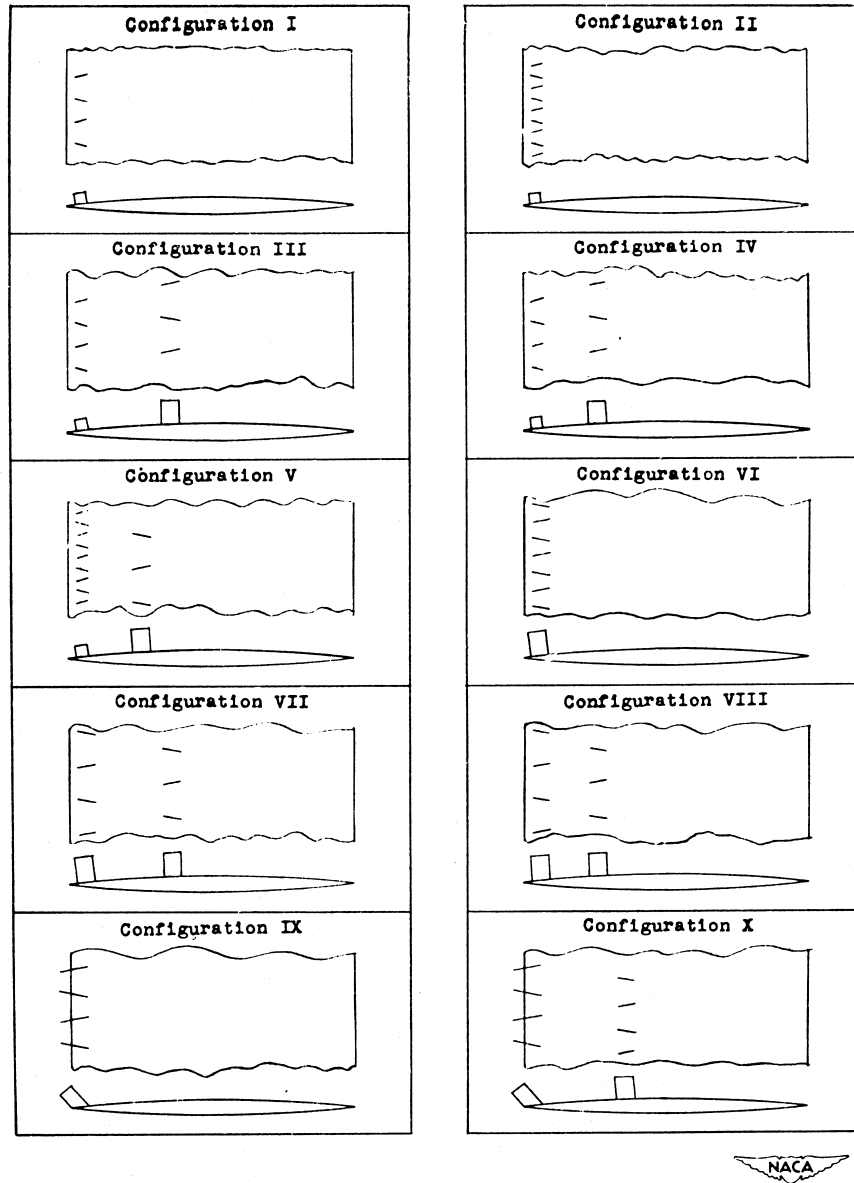


Figure 3.1 Vortex-generator test configurations shown approximately to scale. From Bursnall (1952).

A completely new approach to control the separated flow over wings with sharp leading edges was introduced by Zhou *et al* (1993). Following the theory established in Wu *et al* (1991), they tested a NACA 0025 with its sharp leading edge facing upstream, and a 2.2 percent chord flap on the suction side near the leading edge. It must be noted that the flap oscillation was a mere 0.5-1 mm peak to peak. The tested model can be seen sketched on Figure 3.2.

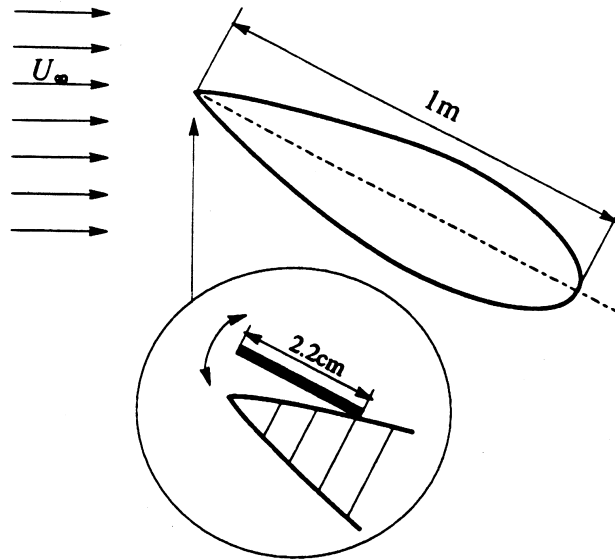


Figure 3.2 Sketch of testing model. From Zhou *et al* (1993).

Zhou *et al* found that at an angle of attack of 27° and with proper frequency, lift was increased by 60-70% in comparison with the stationary configuration. Both balance measurements and pressure distributions were acquired on their experiment. Results are shown in Figures 3.3 and 3.4, where the reduced frequency is given by: $f = f_{flap} \cdot c / U_\infty$. Figure 3.3 shows an increment of 70% for $f = 1$ reducing to 60% for $f = 2$. Zhou *et al* make the comment that at lower angles of attack or lower Reynolds numbers, the forcing effects were smaller, but no results are included. Figure 3.4 shows that when the forcing is imposed, a separated region containing a strong vortex in the upper surface is attained in the mean sense. Reattachment follows close to the trailing edge. Pulsed-wire measurements made possible a deeper insight and confirmed the existence of the vortex capturing.

Hot wire measurements in the wake taken from the paper are shown in Figures 3.5, 3.6 and 3.7. The first figure implies that forcing practically made no change in vortex shedding from the airfoil. Figure 3.6 at the same time, shows a reduction in turbulence intensity in the wake, that is, a reduction of vorticity carried by each vortex shed from the airfoil. This means that forcing did not capture singular vortices but prevented vorticity from

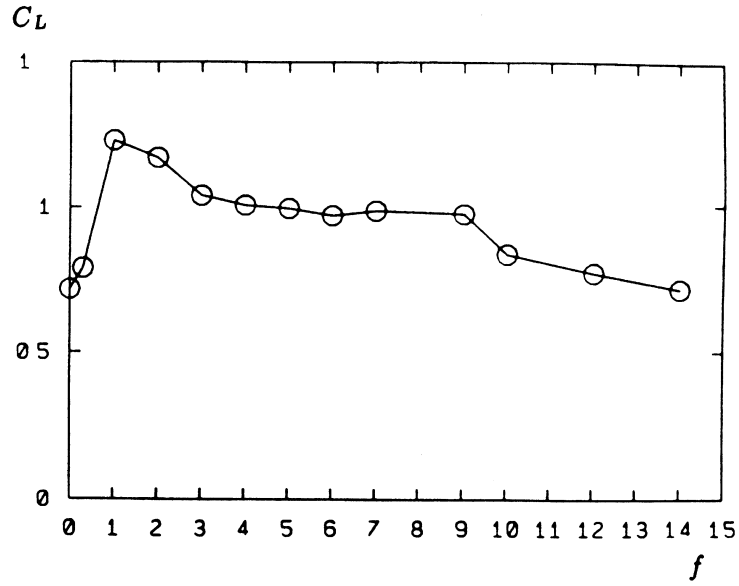


Figure 3.3 Variation of lift coefficient with forcing frequency. $\alpha = 27^\circ$, $Re = 6.65 \times 10^5$.
From Zhou *et al* (1993).

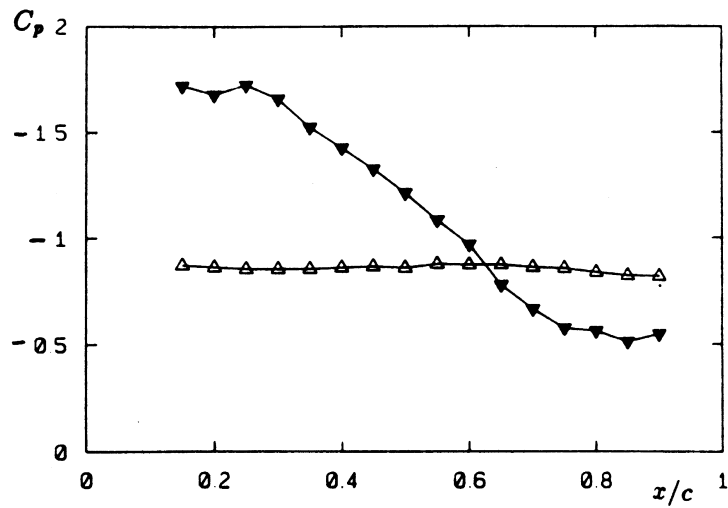


Figure 3.4 Distribution of pressure coefficient. $\alpha = 27^\circ$, $Re = 6.65 \times 10^5$. From Zhou *et al* (1993).

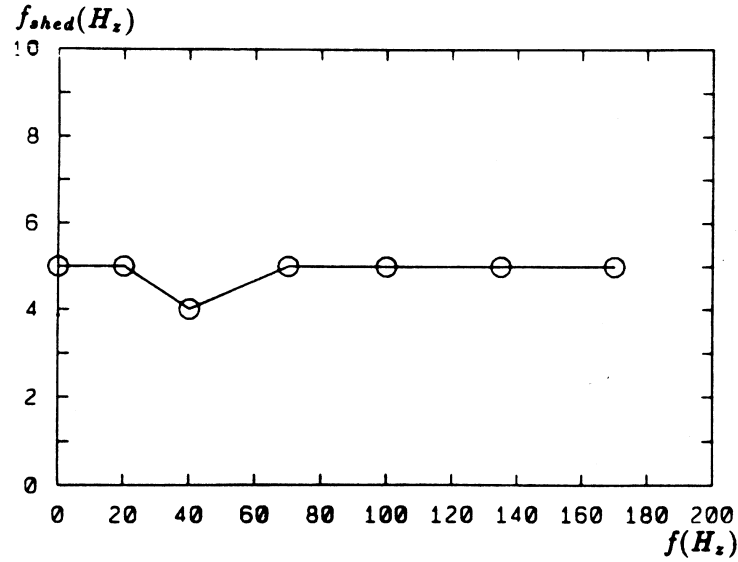


Figure 3.5 Relation between vortex shedding frequency and forcing frequency. $\alpha = 27^\circ$, $Re = 6.71 \times 10^5$. From Zhou *et al* (1993).

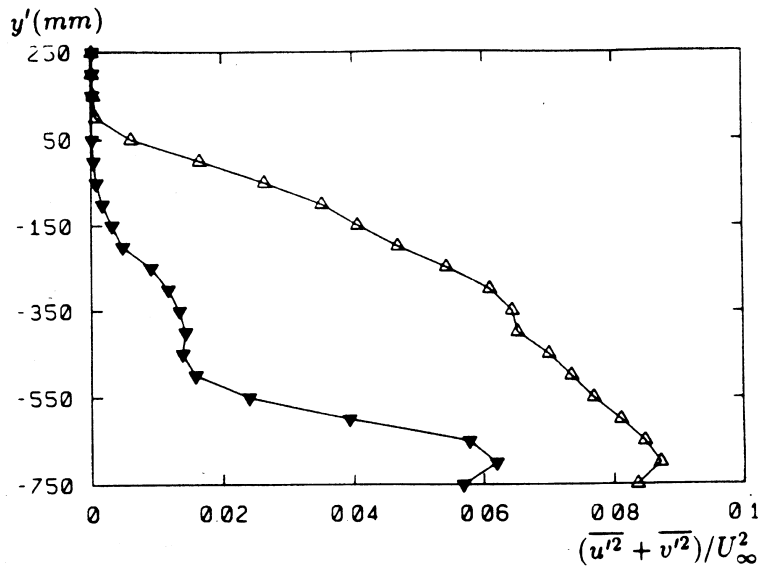


Figure 3.6 Turbulence energy in the wake. y' is the vertical distance in the wind-tunnel coordinates, with $y' = 0$ at the leading edge of the airfoil. $\alpha = 27^\circ$, $Re = 6.71 \times 10^5$, $x/c = 1.615$. Open symbols: unforced; closed: forced with $f = 2$. From Zhou *et al* (1993).

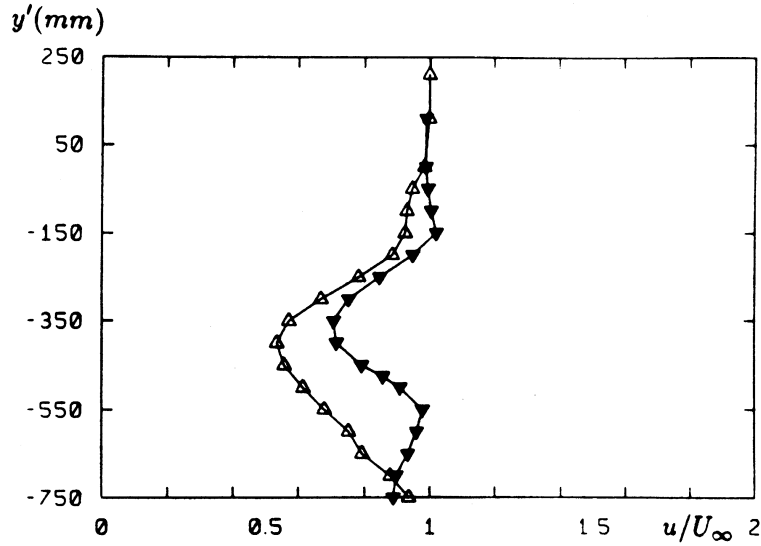


Figure 3.7 Mean velocity profile in the wake. y' is the same as in Figure 3.6, $\alpha = 27^\circ$, $Re = 6.71 \times 10^5$, $x/c = 1.615$, $z/c = 0.15$. Open symbols: unforced; closed: forced with $f = 2$. From Zhou *et al* (1993).

being swept out. The conservation of this vorticity contributed to a time-average large scale vortex on the upper surface, that incremented lift. The last figure depicts a reduction of the mean velocity defect. That translates to the fact that there is drag reduction present as well.

The overall idea gained on this paper is that a huge increase in L/D can be obtained with a small perturbation applied on the shear layer. The average capturing of a vortex on the suction side leads to more than beneficial results.

Another interesting paper on flow control over stalled airfoils applying an oscillating flap actuation is given by Hsiao *et al* (1993). They instrument a NACA 63₃-018 airfoil with a flap mechanism close to the leading edge and study parametrically the effects of position, amplitude and frequency of the flap motion, as well as the Reynolds number at post-stall angles of attack. The angles of attack tested are 28° , 31° and 35° , whereas the Reynolds numbers are $Re = 1.9 \times 10^5$ and $Re = 3.2 \times 10^5$. From the excitation frequency effects, they can deduce that the most effective forcing frequency is that of the natural shedding frequency of the vortical structures in the shear layer. Excitation of the first harmonic, $2f_s$, or the first sub-harmonic, $f_s/2$ does have some effect, but significantly smaller than the fundamental forcing.

Hsiao *et al* can see the same effect of excitation on the flow pattern over the airfoil as Zhou *et al* : shear layer vortices develop into large vortical structures. These structures induce high velocity to lower the pressure on the airfoil upper surface. The long time average of lift can be incremented as much as 50%. Energy spectra of the velocity fluctuations in the wake region, show that when the natural shedding frequency is forced, the fundamental mode attains significantly higher energy while it becomes narrower. This means that the vortical flow pattern becomes more organized due to the effective forcing.

Studies on location and amplitude of the oscillating flap show that both have effects on lift and drag. Moreover, the aerodynamic properties become more sensitive as α increases. They believe that at a high angle of attack the development of the rolled-up vortex is less restricted by the airfoil upper surface. However, efficient control is achieved when the flap protrudes into the shear region to stimulate the unstable shear layer. At angles above 40° their flap extended beyond the shear layer, setting the limit for the actuation system. Amplitude effects proved to be secondary as long as the tip of the flap protrudes the shear layer.

Using the same set up, Hsiao *et al* (1998) studied the effects of the oscillation modes shapes on the aerodynamic properties. Different modes of actuation were tested and are shown in Figure 3.8 along with the experimental arrangement.

The oscillating mode of the flap motion shows to be an important parameter on the final aerodynamic performance. Excitation mode $T_{2,6}$, $T_{3,6}$, or $T_{4,6}$ gives a much better lift coefficient increase than mode S or $T_{2,4}$, whereas mode $T_{2,5}$ falls in between them. At the stalled α the most effective mode, $T_{2,6}$, obtains a 20-45% extra increase of lift coefficient in comparison to mode S . Mode $T_{2,6}$ not only produces a stronger leading-edge vortex, but also causes an earlier vortex formation and a lower vortex convection speed on the vortex-enhancement process.

Hsiao *et al* (1990) applied acoustic excitation of wall-separated flow on the NACA 63₃-018. One-mm-wide slots are located at 1.25%, 6.25% and 13.75% chord to emit acoustic waves coming from a loudspeaker and measure the most effective position. Even when their goal is to delay stall, controlling separation and favoring reattachment, their conclusions and comments are valuable. They perform excitation at different frequency levels in three regions: pre-stalled region, stalled region, and post-stalled region. Lift increase is negligible for the pre-stalled region, but becomes significant as angle of

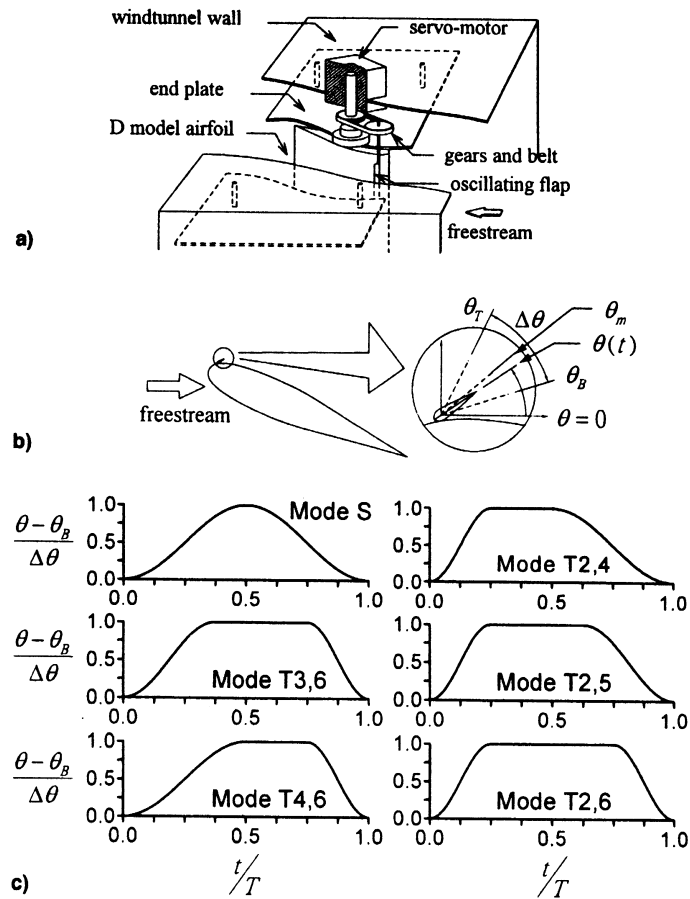


Figure 3.8 a) Schematic of experimental arrangement, b) coordinate system of the flap motion, and c) oscillating mode shapes of the flap motion. From Hsiao *et al* (1998).

attack increases. In the post-stalled region with angles of attack greater than 16° , they found for a $Re = 3.0 \times 10^5$ that lift increments in the order of 40% are attained for the 18° to 22° range and excitation frequencies around 100 Hz. At 24° an increment of 20% in lift is still preserved. The results are shown in Figure 3.9.

Frequencies of excitation used in the experiment are much higher than that of vortex shedding frequencies. The control is being performed at the shear-layer instability frequency rather than at the natural shedding frequency, being an order of magnitude higher than the latter. This interesting fact shows us that in control of flow separation and control of separated flow different order of magnitude frequencies are in play. From the

results, we can see that at higher angles of attack, high frequencies (higher harmonics of the shedding frequency) don't seem to affect the flow considerably.

Forcing location showed to be more effective close to the separation point, especially in the post-stalled region. This is important evidence indicating that the nature of local excitation control is due to hydrodynamical disturbances rather than acoustics. If it were due to acoustics, the forcing should not be sensitive to location. This leads us to conclude that the effect is due to vortex streaming rather than acoustic streaming, or even better, a mixed effect.

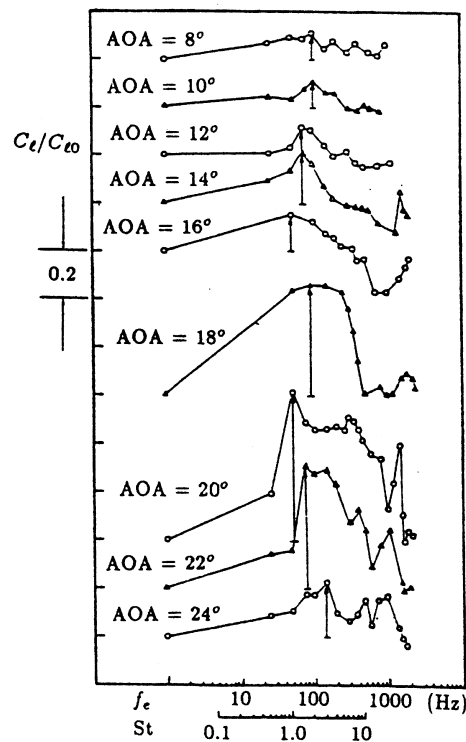


Figure 3.9 Variation of normalized lift coefficients over an airfoil with excitation frequency at different angles of attack for $Re = 3.0 \times 10^5$ and forcing at a 1.25% chord. Arrow indicates bigger C_l/C_{l0} , with the base positioned at $C_l/C_{l0} = 1$. From Hsiao *et al* (1990).

Chang *et al* (1992) investigated this effect, employing the same model and analyzing the forcing level effects on the airfoil performance. The model geometry remained the same, but only one slot of width 0.6 mm placed at 1.25% chord from the leading edge.

Hot-wire velocity measurements were performed at the slot exit at different excitation frequencies. Sound pressure level (SPL) was also measured at the slot exit, and the results showed that the corresponding maximum theoretical acoustic velocity fluctuations were only a small percentage to the measured velocity fluctuations u' . They deduced that this unsteady pulsing of the fluid around the slot is the main disturbance source affecting the flow field around the airfoil, and not the acoustic waves as it was believed.

Figure 3.10 and 3.11 shows relevant results for the non calibrated actuation (u'_{max} is not constant through the frequency forcing spectrum) for two different loudspeakers. It is important to notice that a SPL value of 136 dB is equivalent to maximum acoustic velocity fluctuations of 0.29 m/sec.

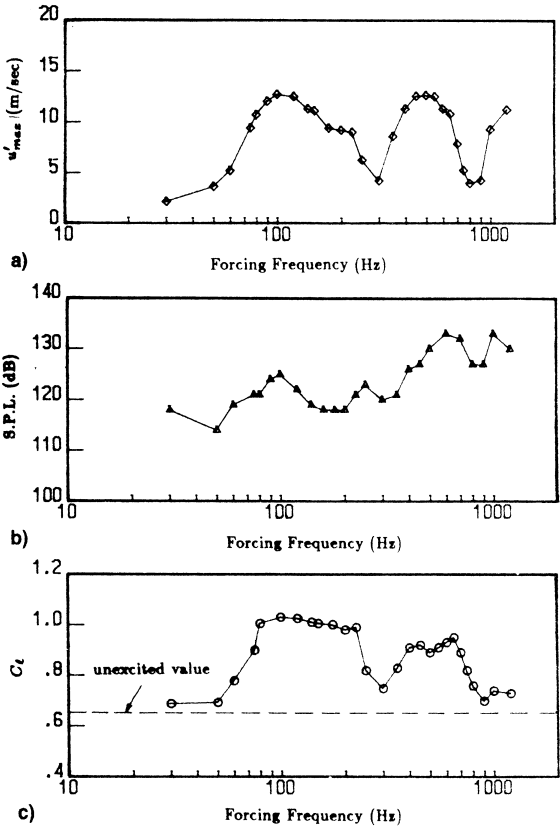


Figure 3.10 a) Maximum velocity fluctuation; b) the corresponding sound pressure level at the slot exit; and c) the lift coefficient at constant driven voltage and AOA = 22°. From Chang *et al* (1992).

Again, the results obtained support the fact that the actuation is more effective when the forcing frequency is “locked-in” to the shear layer instability frequency. This was examined further by Hsiao *et al* (1994), by placing the same model at higher angles of attack, to the high post-stall angles ($> 24^\circ$). He noted that for the low post-stalled region ($20^\circ - 24^\circ$) there is an absence of well-defined peaks in the airfoil wake frequency spectrum, showing that no significant vortex structure has formed behind the airfoil. At higher angles, narrow banded peaks are present due to the vortex shedding formation. In

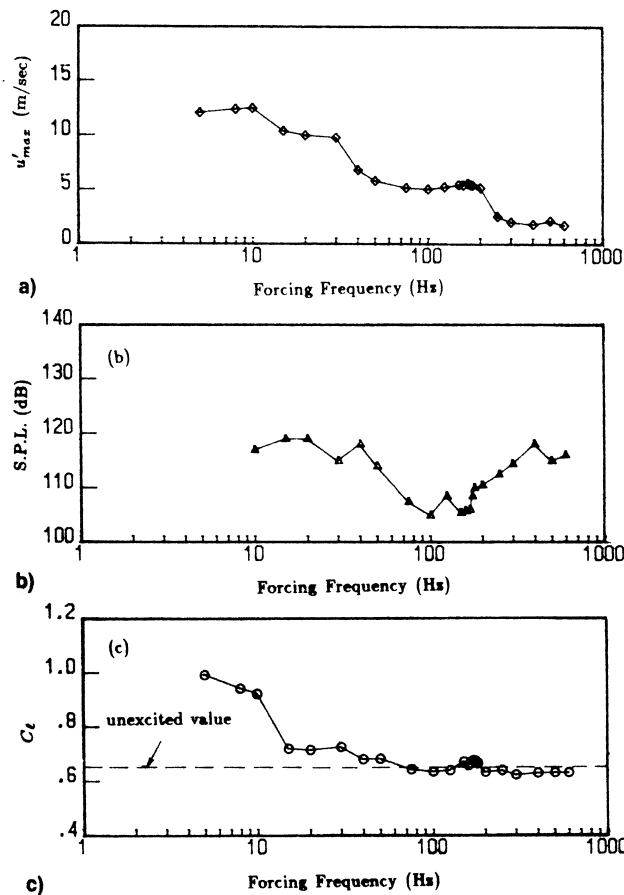


Figure 3.11 a) Maximum velocity fluctuation; b) the corresponding SPL; and c) the lift coefficient at $AOA = 22^\circ$ and driven by a low-frequency loudspeaker. From Chang *et al* (1992).

this regime, they found that the most effective frequency for improving aerodynamic performance is correlated to the vortex shedding instability frequency in the wake. Under

excitation conditions, leading edge separation still occurs and with the flow remaining detached to the airfoil surface, in contrast to the low post-stall regime. Pressure distribution results are shown in Figure 3.12.

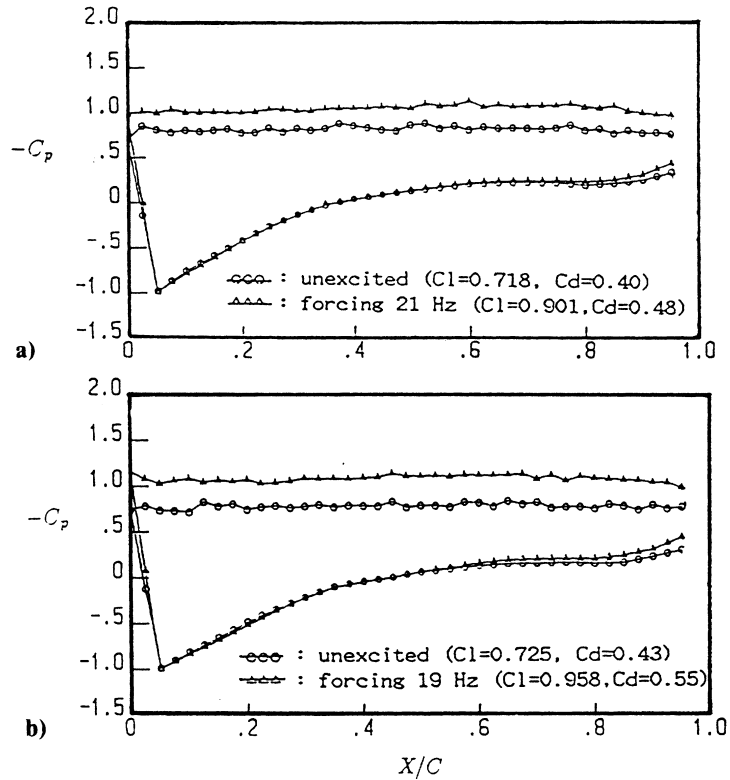


Figure 3.12 Airfoil pressure distributions with and without excitation for angles of attack :
 a) 26° and b) 28° . From Hsiao *et al* (1994).

Of course, the work of Hsiao *et al* (1990), Chang *et al* (1992) and Hsiao *et al* (1994) indicates that acoustic excitation of separated flow is really an alternative term for the modern definition of synthetic jets. Crook *et al* (1999) gives one of many contributions to the development of this new devices. A synthetic jet device consists of a cavity with rigid side walls, an oscillating wall and a rigid cap with an orifice. A schematic is shown in Figure 3.13.

Synthetic jets derive their name from the fact that they synthesize a jet from a train of vortex rings or pairs, formed from the external fluid surrounding the orifice, without net mass addition. In Crook's paper, it is also mentioned that a loudspeaker in a cavity was a

usual form of creating synthetic jets. It is important to note that the sharp edges on the orifice may contribute through acoustic streaming to the formation of the jet without net mass flow.

Crook *et al* (1999) performed some preliminary control of the separation of the turbulent boundary layer on a circular cylinder, with a single jet positioned just upstream (93.5 degrees) of the separation point. The device was driven at the natural shedding frequency, and fluid flow visualization was used to check the effectiveness. The synthetic jet creates a very strong entrainment of the surrounding fluid, and also penetrates the boundary layer. They observed a delay in the separation line, even when only one device is used.

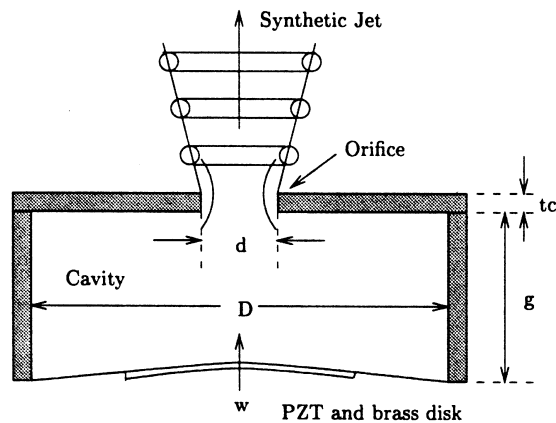


Figure 3.13 Schematic diagram of a synthetic jet. From Crook *et al* (1999).

A more graphical visualization of the entrainment produced by a synthetic jet is given in Kiya *et al* (1999). They performed flow control over a stalled flat plate at an angle of attack of 10° by introducing vortex rings into the separated layer. The rings were produced through an orifice of 5 mm bored through the top wind tunnel wall, which was connected to a woofer through a chamber. Figure 3.14 clarifies the set-up.

Results show that the vortices in the shear layer interact with the vortex ring yielding a local increase of moment thickness, thus increasing the entrainment rate. A compact rolling up vortex is created that eliminates the reverse flow on its downstream side, by transporting high momentum fluid of the main flow towards the surface. This

generates a dynamic reattachment moving from $x/c = 0.4$ to $x/c = 0.8$, reducing the separation zone.

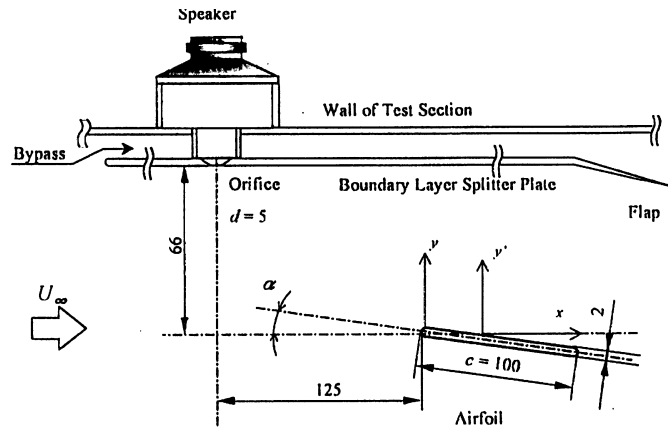


Figure 3.14 Experimental set-up for active control of stalled flow around an airfoil by impinging vortex rings. From Kiya *et al* (1999).

For this low Reynolds number case (8300), the most effective frequency happens to be approximately half of the Kelvin-Helmholtz instability. But at higher Reynolds numbers, the primary mechanism to determine the optimum frequency is the shedding-type instability. Figure 3.15 presents a sequence of a vortex impinging the plate shear layer.

Computational Fluid Dynamics (CFD) makes important contributions to the knowledge of fluid behavior. A paper reflecting the importance of numerical simulations to post-stall flow control is given by Wu *et al* (1998). In this paper, the authors perform Reynolds-averaged two dimensional computations of turbulent flow over an NACA 0012 airfoil at post-stall angles of attack, including periodic blowing-suction excitation located at the 2.5% of the chord.

The authors show that massively separated and disordered unsteady flow can be effectively controlled by a local unsteady excitation, with low-level power input. The unforced random separated flow under proper excitation frequency, becomes periodic or quasi-periodic. This is associated with a strong lift enhancement. They also show that in some situations reduction of drag and pressure fluctuations (i.e.: buffeting) is possible.

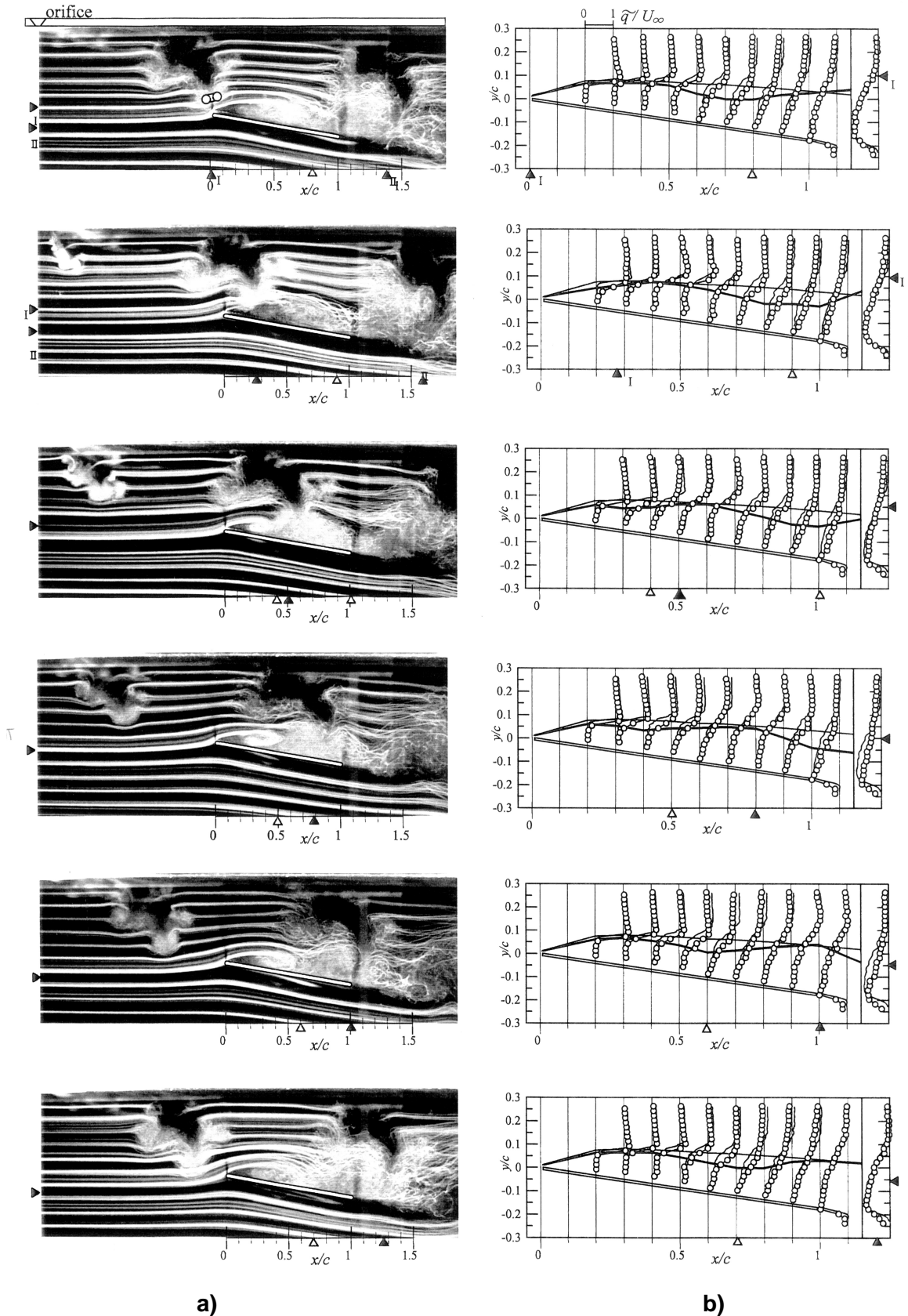


Figure 3.15 For caption, see below. Taken from Kiya *et al* (1999)

Figure 3.15 a) Flow visualization of the separated flow affected by the impinging vortex rings. Flow is from left to right. The phase-averaged reattachment position is indicated by the open triangles. Coordinates of position of the vortex rings are denoted by the solid triangles on the x and vertical y axes; b) Phase-averaged velocity distributions \bar{q} in the separated flow affected by the impinging vortex rings. The phase-averaged reattachment position is indicated by the open triangles. Coordinates of position of the vortex rings are denoted by the solid triangles on the x and y axes. Thin solid lines indicate the distributions of the time-averaged velocity \bar{q} in the undisturbed shear layer, while the solid lines show the center of the shear layer.

It's interesting to notice that they focus their attention on the control of the leading edge shear layer, for its upstream location, highly flexible receptivity, and being the only source of vortex lift.

The most effective actuation frequencies were the natural shedding frequency, and its subharmonics and superharmonics, for angles of attack from 18° to 35° . Lift enhancement up to 70% was achieved, and random high frequency modes were shown to be almost suppressed in some cases ($f = 2f_s$), implying a perfect frequency *lock-in*. This is reflected in Figures 3.16 and 3.17.

Wu *et al* (1998) also explored the physical mechanisms in terms of nonlinear mode competition and resonance, as well as vortex dynamics, ending with significant conclusions. They point out that forcing with proper frequency and amplitude can cause the response frequencies of both shed vortices and shear layer to lock into the harmonics of the forcing frequency, suppressing other modes. This leads to a well organized flow that from the vortex-dynamics point of view corresponds to a sufficiently strong entrainment due to the rolling-in structure of the lifting vortex. To create this vortex, two conditions must be met. First, the discrete vortices in the shear layer must be forced into rolling-up coalescence, possible only if the forcing frequency is an order of magnitude lower than the natural shear-layer frequency, and the forcing amplitude is above a minimum. Second, the concentrated lifting vortex must be not too far from the airfoil surface, To ensure this conditions, the angle of attack cannot be too close to stall neither too large.

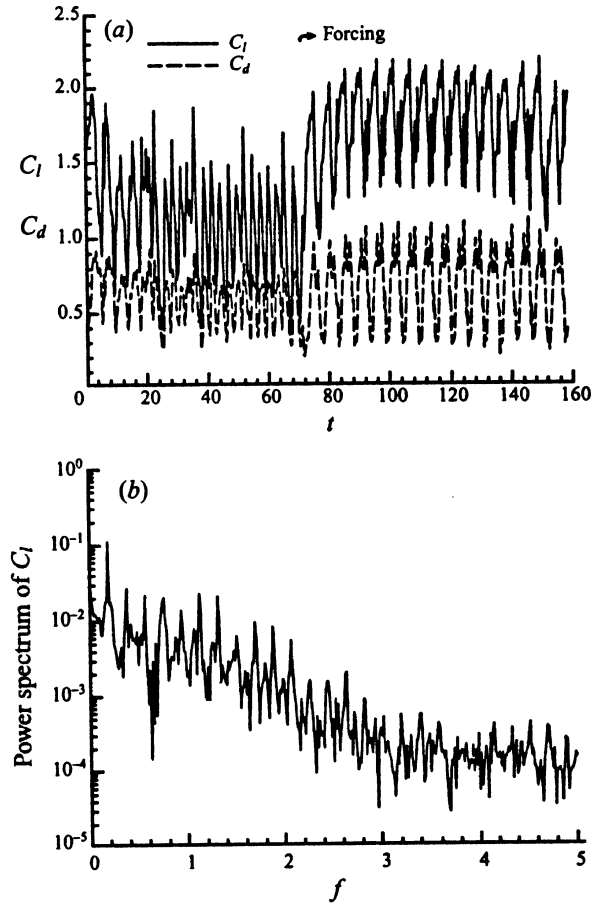


Figure 3.16 $f_a/f_s = 0.5$, $C_m = 2.5\%$, with $C_m = |v|_{max} l/U_\infty c \sin \alpha$ being $l = 2.5\% c$ and $|v|_{max}$ the maximum perturbation velocity. a) Instantaneous lift and drag coefficients. b) Power spectral density of C_l .

He *et al* (2000) also repeated computations on a post-stalled NACA 0012. The excitation was performed with both steady blowing and synthetic jets. Some discrepancies exist between the two papers, showing that more computation validation is needed and a benchmark for this kind of flow field is still far from being obtained. More research in both experimental and computational fields needs to be accomplished. However, the results confirm that steady blowing is not an effective tool for deep stall flow control. An interesting point, is the fact that they tried to control high angle of attack flow placing a jet on the pressure side close to the trailing edge, although the actuation used was steady blowing ending with almost no increase in lift.

Another important difference to Wu *et al* (1998) is their conclusion that even when forcing frequency may improve the averaged lift, it also increases the pressure oscillation amplitudes.

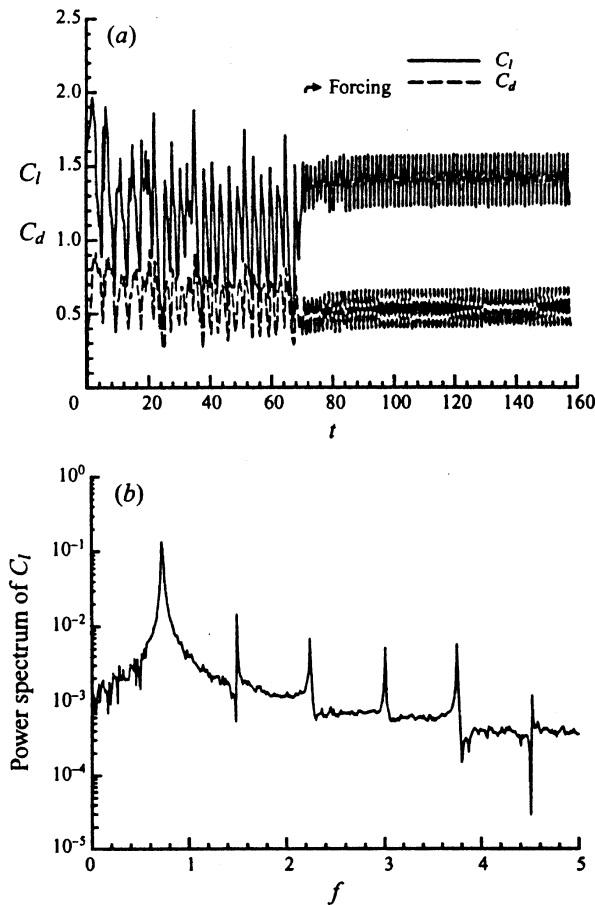


Figure 3.17 As Figure 3.16 but $f_a/f_s = 2$.

3.2 Conclusions

It is not difficult to conclude that in order to capture a vortex in the average sense over the airfoil suction side, an efficient way to periodically perturb the leading edge shear layer is needed. For that reason, the actuation system selected for the current research is the same as the one utilized by Zhou *et al* (1993) in their experiment. Even more, the idea of the flap working as a synthetic jet seems reasonable. If properly sealed and actuating

from the fully closed position to a certain angle, flow suction and blowing should occur by while the flap is moving. This comes from a simple analysis supported by the principle of conservation of mass in the cavity generated between the flap and airfoil. Neither of the papers dealing with flaps as the mean of actuation fully investigated the effect of the flap in the shear layer.

All the papers but one (He *et al*, 2000) focus their control to the leading edge shear layer. The actuation of the trailing edge shear layer may also affect the flow through its global instability. This is one of the points to be studied in the present experiment.